Level Set Segmentation Based on the Prior Shape of Biological Feature

Ji Zhao(✉), Dongxu Ji, and Yuxiang Feng

School of Computer Science and Software Engineering, University of Science and Technology, Anshan 114051, Liaoning, China

Abstract. The identification of user's identity which is based on the analysis and measurement of the biological characteristics has become a research hotspot. The precise location and segmentation of the target is the basis for accurate biometric recognition. In view of the similarity of the external shape of human biological characteristics, the prior shape knowledge is introduced into active contour model based on level set. First, the training data of the shape function, which is expressed by the level set, are projected onto a lower dimensional subspace and achieved the primary attribute reduction on approximately Gaussian distribution of the training set using PCA method. Second, the further optimized properties are obtained by minimization class attribute interdependence minimization (CAIM) algorithm. Finally, under the constraints of the prior shape and object personality traits, level set curve based on the border and region can accurately evolve into the target boundary. Experiments demonstrate that our model can cope with image noise and clutter, as well as partial occlusions.

Keywords: Pattern recognition · Image processing technology · Image segmentation · Level set method · Prior shape

1 Introduction

In the field of computer science and technology, the biometric identification technology [1, 2] by analyzing and measuring the physiological characteristics of the human body has become a research hotspot. Compared with the traditional identification method, the biometric identification technology has the advantages of safety, reliability, not easy to forget, good security performance, not easy to be stolen and portability, and can be used at anytime and anywhere. The technology can be widely used in government, military, banking, social security, electronic commerce, security and defense [3]. Currently, the biometric features used for identification include fingerptints, iris, face, voice, palm, hand shape, retina, ear shape, etc.

The foundation of biometric identification is the segmentation and localization of the features. Due to the complexity of the background, the blurred edge and the defect of target, the segmentation method can not get the desired segmentation results. The main reason is that the low level gray information of the image can not fully express

H. Song and D. Jiang (Eds.): SIMUtools 2020, LNICST 369, pp. 651–666, 2021.
https://doi.org/10.1007/978-3-030-72792-5_51

the characteristics of the target [4]. The method of solving this problem is to introduce the prior information of object such as color and shape into the evolution of the curve in the segmentation model. We can use curve evolution global geometric features and the local shape features of object to effectively deal with occlusion, noise and target shape changes in image segmentation. The parametric shape modeling methods include distance mapping [5], snake line model with elastic properties [6], template method [7], and skeleton method [8]. Although these methods can effectively describe local deformation, but a large number of parameters is required and they can not handle topological shape change. So we use the level set method to overcome the parametric shape model shortcomings [10]. First, a shape model, which is constructed by using a set of samples in the level set space, is used to describe the change of a priori shape by variational framework. And then, the prior shape term is introduced into the level set energy model.

At present, the research of level set segmentation model based on shape a priori information has made some progress. Leventon M E, Grimson W E L and Faugeras O [9] established shape prior statistical model by using linear principal component analysis (PCA) method in shape training set. Rousson M and Pragios N [10] put forward the implicit expression of the level set model by integrating shape prior information into the regional information. Pan B, Wang W, Yan J, et al. [11] propose a level set model, which incorporates shape priors and the gradient information of the image into C-V model for prostate MRI segmentation, and can segment the prostate contour in MRI with high precision. Cremers D, Tischhauser E, Weickert J [12] combined the geodesic active contour model and the prior shape with kernal to guide curve evolution. Cremers D, Sochen N and Schnorr C [13] proposed tag function to make a fixed template and priori shape integrated with pose information. Karantzalos K and Paragios N [14] can automatically analyze the number and angle of target objects by integrating a priori information of different shapes, and then they proposes a 3D automatic reconstruction method of remote sensing data based on variational farmework [15], which solves the segmentation problem of optical images and digital elevation maps, and determines their positions and 3D geometric shapes based on prior knowledge.

2 Related Work

In terms of shape description, the level set model is used to present the shape features. First, it is an implicit and intrinsic measure of expression and can automatically deal with the changes in the topology. Secondly, it provides a natural way to estimate shape geometric properties such as curvature and normal vector. Typically, the level set function is often defined by the distance function in the image space. This form of expression is consistent with the level set model of curve evolution, therefore it can be naturally fused to the active contour segmentation framework.

Each curve in the training set is regarded as the zero level set on the high dimensional surface. It is the goal that shape modeling is to find the probability distribution of these surfaces. Since they all describe the shape of the same kind of object, the curves of the training set are dependent on each other. So it is inevitable to leads to more redundancy in the training set. It can be considered that the object shape approximately obeys multidimensional Gauss distribution and the shape changes are mainly concentrated in the

vicinity of the mean shape. Firstly, the new algorithm applys principal component analysis method to training set for rough extraction, which can get the data mainly affecting the shape modeling. After the PCA process the class attribute interdependency minimum (CAIM) method is used for data optimal reduction. In the image feature descriptor dimensionality reduction the combination plays an effective role, which removes the contents of the original descriptor redundancy, and also fully retains the important data.

Since CAIM algorithm is mainly related to attribute combination entropy and the attribute dependence entropy of the sample set, it can extract data with the more typical contribution and reduces the data with no typical contribution to improve the expression of prior shape.

2.1 Primary Feature Extraction Using PCA Method

Cootes T and Taylor C [16] proposed PCA to set up the parameters contour model to segment the different objects. Leventon M E, Grimson W E L and Faugeras O [9] applied the PCA to symbols distance function (SDF) in geometry contour model. In comparison, SDF has a greater tolerance than the parameterized contour and improves the robustness, accuracy and speed. The signed distance function of sample set is $\phi = \{\phi_1, \phi_2, \cdots, \phi_n\}$, where n is the number of training samples, can be calculated as:

$$\overline{\phi} = \frac{1}{n} \sum_{i=l}^{n} \phi_i \tag{1}$$

The mean shift is obtained by subtracting the mean value from each sample.

$$\hat{\phi}_i = \phi_i - \overline{\phi}, \quad i = 1, 2, 3, \cdots, n \tag{2}$$

The adjustment of the data structure is carried out to each mean shift. First, the mean shift is adjusted to the column vector of $(m \times l) \times 1$ from the original $(m \times l)$ matrix, and each column vector is combined together to form a new matrix $X\,(n(m \times l))$, where m, l are the sample image column width and row height. Secondly, we calculate the covariance between two columns of the X to form a covariance matrix $M\,(n \times n)$. Finally, the singular value decomposition of M is defined as:

$$M = U \Sigma \Lambda \tag{3}$$

where U is the feature vectors matrix of M, Σ is a diagonal matrix whose diagonal elements are eigenvalue $\Lambda = \{\lambda_1, \lambda_2, \cdots, \lambda_n\}$ of M. Then, the feature vectors are sorted according to the corresponding eigenvalues. Finally, the eigenvalue E of X is

$$E = XU = (e_1, e_2, \cdots, e_n) \tag{4}$$

After getting the feature vector of X, the regularization is needed. Thus the number of feature vectors is determined as follows:

$$Fd = \frac{SUM_k}{SUM_n} \tag{5}$$

where the symbol SUM_i is the sum of the former i eigenvalues and k < n. The final step in the principal component analysis is the reconstruction of the data. Given characteristic coefficient $\lambda^k_{pca'}$, the new signed distance function is calculated.

$$\hat{\phi} = Ek\lambda^k_{pca} + \overline{\phi} \tag{6}$$

where the characteristic coefficient λ^k_{pca} is the weight coefficient of k change mode. Obviously, when λ^k_{pca} is zero, the mean value of the sample is obtained.

2.2 Attribute Reduction Based on Clustering Theory

Class Attribute Dependency Minimization Algorithm. Class attribute dependency minimization algorithm is mainly about the feature combination property and mutual interdependence relationship of feature patterns as well as formulation of the concept of typicality and diversity for data set [17]. Its targets are as follows:

- Through statistical filtering and feature being reattached weight value, we get the limited possible solutions in feature combination property and mutual interdependence relationship.
- Based on the estimation of the set entropy and mutual entropy, the model of feature combination property and mutual interdependence relationship is defined.
- An algorithm, which can be used to improve the inherent patterns and simplify the sample data, is proposed to reduce the uncertain sample data with deviation from the set Class attribute dependency minimization algorithm.

Ensemble Entropy Estimation. Given a finite set of n samples X, $Xi(i = 1, 2, \cdots, n)$ is a discrete random set $a_{i1}, a_{i2}, \cdots, a_{im}$ and a_{ij} is the jth observation variables of the ith sample. Matrix $A = aij|i = 1, \cdots, n; j = 1, \cdots, m$ is called the observation matrix of the set X. Therefore, the row vector $Xi = [a_{i1}, a_{i2}, \cdots, a_{im}]$ is a collectionof m observation variables about the first i samples, and the column vector $Y_{j'} = \left[a_{1j}, a_{2j}, \cdots, a_{nj}\right]$ is the collection of n samples for the first j observation variables. Some definitions are as follows:

- Definition 1: $\omega = \omega_1, \omega_2, \cdots, \omega_n$ is defined as weights of a n-dimensional vector set, in which ωi corresponds to the weight of the first i vector, and $\sum_{i=1}^{n} \omega_i = 1$.
- Definition 2: Based on ω, the estimated probability on Y is defined as:

$$p^k_j(\omega) = \sum\nolimits_{i=1}^{n} \delta^k_{ij}\omega_i \tag{7}$$

where

$$\delta^k_{ij}(\omega) = \begin{cases} 1, |a_ij - a_kj| < \varepsilon \\ 0, |a_ij - a_kj| \geq \varepsilon \end{cases} \tag{8}$$

where, $k = 1, 2, \cdots, L_j, j = 1, 2, \cdots, m$. $\varepsilon(\varepsilon \geq 0)$ is a very small number relative to attribute values. L_j is the length of the j observation variable, the $p^k_j(\omega)$ is the p^k_j in the case of a given ω.

- Definition 3: The combination entropy of an observed variable Yj is:

$$H(j) = -\sum_{k=1}^{L} p_j^k \log p_j^k \tag{9}$$

- Definition 4: The $\binom{m}{2}$ finite schemes for all events in X is defined as:

$$\left\{ p_{ij}^{kl} \middle| k = 1, 2, \cdots, L_j; \quad l = 1, 2, \cdots, L_{j'}; \quad j, j' = 1, 2, \cdots, m; \quad j' > j \right\} \tag{10}$$

- Definition 5: The mutual interdependence entropy between Y_j and $Y_{j'}$ is defined as:

$$H\left(j, j'\right) = -\sum_{k=1}^{Lj} \sum_{l=1}^{Lj} q_{jj'}^{kl} \log q_{jj'}^{kl} \tag{11}$$

- Definition 6: The $\binom{m}{2}$ finite schemes for all events in X is defined as:

$$R_{jj'}^{(2)} = \frac{I\left(j, j'\right)}{H(j, j')} \tag{12}$$

where, $I\left(j, j'\right) = H(j) + H\left(j'\right) - H\left(j, j'\right)$, and $0 \le R_{jj'}^{(2)} \le 1$, if $R_{jj'}^{(2)} = 0$, the Yj and Yj' are completely independent, if $R_{jj'}^{(2)} = 1$, the two features are completely dependent. And if

$$R_{jj'}^{(2)} \ge \frac{X^2 (Lj - 1)\left(Lj' - 1\right)}{2nH(j, j')} \tag{13}$$

it is showed that there is some dependencies between features Y_j and $Y_{j'}$.

3 A Variational Level Set Segmentation Model Based on Prior Shape Information

The energy functional for the variational level set model for image segmentation is

$$E(u) = \mu E_c + \alpha E_e + \beta E_R + \lambda E_S \tag{14}$$

where E_c is the energy functional corresponding to the constraint term of the signed distance function, E_e is an energy functional based on edge, E_R is an energy functional based on region, and E_s is an energy functional of priori shape. E_c, E_e, E_R and E_S are defined as respectively:

$$Ec = \frac{1}{2} \int_{\Omega} (|\nabla u| - 1)^2 dxdy \tag{15}$$

$$Ee = \int_{\Omega} g\delta(u)|\nabla u| dxdy \tag{16}$$

$$E_R = \int_{\Omega} \lambda_1 H(u) dxdy + \int_{\Omega} \lambda_2 (1 - H(u)) dxdy \tag{17}$$

$$ES(u) = \int_{\Omega} \rho(r(X)) H(u) dxdy \tag{18}$$

where

$$r(X) = Su(x) - uG\left(\hat{X}\right) \tag{19}$$

$$\hat{X} = SRX + T \tag{20}$$

The final energy functional can be written as:

$$\begin{aligned} E(u) &= \tfrac{1}{2}\mu \int_{\Omega} (|\nabla u| - 1)^2 dxdy + \alpha \int_{\Omega} g\delta(u)|\nabla u| dxdy + \beta_1 \int_{\Omega} \lambda_1 H(u) dxdy \\ &+ \beta_2 \int_{\Omega} \lambda_2 (1 - H(u)) dxdy + \lambda \int_{\Omega} H(u) \left(ku(X) - uG\left(\hat{X}\right)\right)^2 dxdy \end{aligned} \tag{21}$$

The optimal solution of the energy function $E(u)$ is the stable solution of PDEs as follows:

$$\begin{cases} \frac{\partial u}{\partial t} = u\left(\Delta u - div\left(\frac{\partial u}{|\nabla u|}\right)\right) + \delta\varepsilon(u) \begin{bmatrix} \beta div\left(g\frac{\nabla u}{|\nabla u|}\right) - \beta_1\lambda_1(I - c_1) \\ +\beta_2\lambda_2(I - c_2) - \lambda(Su - uG)^2 \end{bmatrix} \\ -\gamma H(u) S(Su - uG) \quad in\ (0, \infty) \times \Omega \\ \frac{\partial u}{\partial \vec{n}} = 0 \quad on \quad \partial\Omega \\ u(0, x, y) = u0(x, y) \quad in \quad \Omega \end{cases} \tag{22}$$

$$\frac{\partial S}{\partial t} = -\int_{\Omega} H(u)\left(Su - uG\left(\hat{X}\right)\right)\left(u - \nabla_{\hat{X}} uG \nabla_S \hat{X}\right) dxdy \tag{23}$$

$$\frac{\partial(\theta, T)}{\partial t} = \int_{\Omega} H(u)\left(Su - uG\left(\hat{X}\right)\right)\left(\nabla_{\hat{X}} uG \nabla_{(\theta,T)} \hat{X}\right) dxdy \tag{24}$$

Through introducing parameter robust estimation model function $\rho(r)$ and $\phi(r)$, the corresponding equation is rewritten as

$$\begin{aligned} &\tfrac{\partial u}{\partial t} = u\left(\Delta u - div\left(\tfrac{\nabla u}{|\nabla u|}\right)\right) + \delta_{\varepsilon}(u)\left[\alpha div\left(g\tfrac{\nabla u}{|\nabla u|}\right) - \beta_1\lambda_1(I - c_1) + \beta_2\lambda_2(I - c_2) - \lambda\rho(r(X))\right] \\ &-\gamma H(u)\phi(r) S \end{aligned} \tag{25}$$

$$\frac{\partial S}{\partial t} = -\int_{\Omega} H(u)\phi(r)\left(u - \nabla_{\hat{X}} uG \nabla_S \hat{X}\right) dxdy \tag{26}$$

$$\frac{\partial(\theta, T)}{\partial t} = \int_{\Omega} H(u)\phi(r)\left(\nabla_{\hat{X}} uG \nabla_{(\theta,T)}\right) dxdy \tag{27}$$

where respectively S, θ, T is the scaling factor, the rotation factor and the translation.

4 Experimental Results and Analysis

4.1 Segmentation of Human Body Contour

The Acquisition and Expression of Shape Training Set. The shape of body is segmented from 100 representative human images, which constitute a initial training set for priori shape. The eigenvalues of each training data are shown in Table 1. After PCA with fitting coefficient 0.98 attribute reduction, the remaining 27 items are the data of main factor in shape training set, and the eigenvalues of the remaining 27 data are shown in Table 2. And then the optimization of CAIM ($\varepsilon = 0.0008$)is carried out, as shown in Table 3, the 9 feature data are the main contribution to the expression of human body shape, which are selected to construct the priori shape.

Table 1. Eigenvalues of the training set's eigenvectors.

No.	Eigenvalue	No.	Eigenvalue	No.	Eigenvalue	No.	Eigenvalue	No.	Eigenvalue
1	170423.7500	2	138281.4844	3	63030.2813	4	51409.2266	5	39550.5977
6	25377.2617	7	22697.7891	8	15312.2451	9	11525.0322	10	8051.1055
11	6576.4102	12	4771.3081	13	4237.4751	14	3910.4451	15	3238.6929
16	2523.8118	17	2492.7739	18	1826.8881	19	1783.8018	20	1402.3051
21	1498.5015	22	1320.5691	23	1145.8143	24	992.4016	25	960.4662
26	863.5479	27	799.8417	28	682.5350	29	652.1017	30	598.7137
31	567.9088	32	525.1431	33	464.2548	34	460.5003	35	430.3991
36	409.0725	37	369.0485	38	359.8156	39	344.1356	40	337.6111
41	276.9188	42	271.2017	43	249.0898	44	234.0920	45	224.4437
46	210.7977	47	202.8804	48	198.6955	49	177.0910	50	171.4283
51	161.3509	52	151.3801	53	145.2543	54	137.7306	55	135.2908
56	127.0296	57	114.8879	58	111.2170	59	107.5084	60	104.4107
61	99.6913	62	93.6221	63	92.1430	64	84.7209	65	82.2678
66	80.8714	67	75.4714	68	70.7329	69	65.9291	70	63.9189
71	61.1338	72	58.2500	73	56.4961	74	52.8481	75	49.7694
76	48.3934	77	46.5804	78	44.9886	79	43.9146	80	42.1723
81	40.8940	82	0.0330	83	39.5448	84	38.2734	85	36.1238
86	34.7594	87	33.1616	88	31.2365	89	29.0265	90	12.4005
91	27.0900	92	14.1955	93	15.4931	94	16.7723	95	17.5104
96	19.2162	97	23.7321	98	22.9521	99	21.9240	100	19.9770

In order to illustrate the process of establishing training set, we selected a training subset which contains 14 images from the training set to elect binary image of the samples, the results are shown in Fig. 1.

Table 2. Eigenvalues after PCA reduction

No.	Eigenvalue	No.	Eigenvalue	No.	Eigenvalue	No.	Eigenvalue	No.	Eigenvalue
1	170,423.7500	2	138281.4844	3	63030.2813	4	51,409.2266	5	39550.5977
6	25,377.2617	7	22697.7891	8	15312.2451	9	11,525.0322	10	8051.1055
11	6,576.4102	12	4771.3081	13	4237.4751	14	3,910.4451	15	3238.6929
16	2,523.8118	17	2492.7739	18	1826.8881	19	1,783.8018	20	1402.3051
21	1,498.5015	22	1320.5691	23	1145.8143	24	992.4016	25	960.4662
26	863.5479	27	799.8417						

Table 3. Eigenvalues after CAIM optimization

No.	Eigenvalue	No.	Eigenvalue	No.	Eigenvalue	No.	Eigenvalue	No.	Eigenvalue
2	138281.4844	6	25377.2617	7	22697.7891	9	11525.0322	12	4771.3081
12	2492.7739	21	1498.5015	23	1145.8143	24	992.4016		

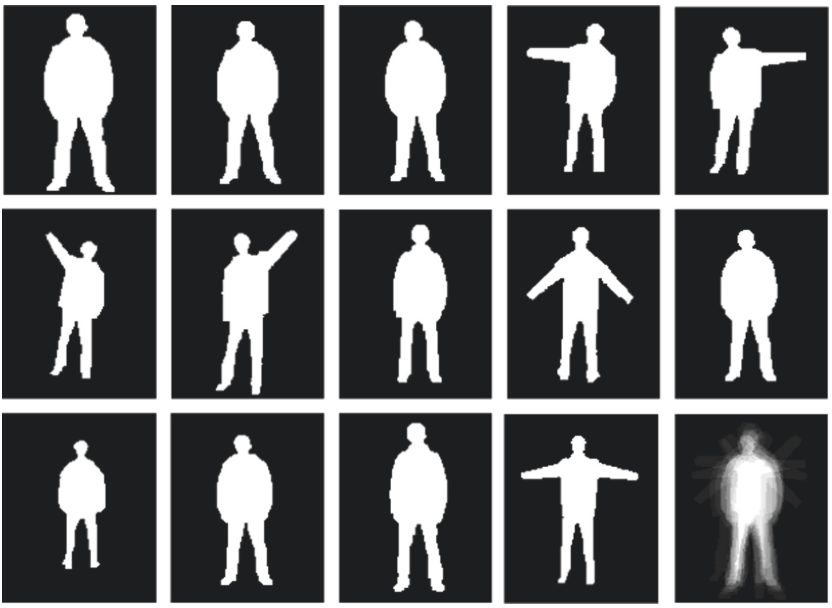

Fig. 1. Original human contour

In Fig. 1, the last image is a superposition of 14 images. As we can see, the overlapped area is relatively small, and the surrounding is fuzzy, which shows that the distribution of information in the image is dispersed.

Registration of Shape Training Set. Binary image registration operation includes three parts: translation, scaling and rotation.

Translation: The translation parameters is determined by object centroid coordinates, the centroid coordinates of binary image *Ik* can be calculated as

$$x^k = \frac{\sum_{i=1}^{m}\sum_{j=1}^{n} x_i I_k(x_i,y_i)}{\sum_{i=1}^{m}\sum_{j=1}^{n} I_k(x_i,y_i)},\ y^k = \frac{\sum_{i=1}^{m}\sum_{j=1}^{n} x_i I_k(x_i,y_i)}{\sum_{i=1}^{m}\sum_{j=1}^{n} I_k(x_i,y_i)} \tag{28}$$

where $k = 1, 2, \cdots, 14$, m and n, respectively, is the number of rows and columns, (x_i,y_i) is the coordinates of the pixel.

Scaling: The zoom scale is measured by the average distance from the edge point of image to centroid. Assume that the edge point coordinate is $\left(x_i^k, y_i^k\right)$, $i = 1, 2, \cdots, M^k$, M^k is the length of the target contour of the k image, the mean distance is defined as:

$$S^k = \frac{1}{M^k}\sum_{i=1}^{M^k} D\left(\left(x_i^k, y_i^k\right), \left(x^k, y^k\right)\right) \tag{29}$$

where $D\left(\left(x_i^k, y_i^k\right), \left(x^k, y^k\right)\right)$ is the Euclidean distance between points $\left(x_i^k, y_i^k\right)$ and point $\left(x^k, y^k\right)$.

Rotation: The rotation angle can be defined as:

$$\theta = \tan^{-1}\frac{\Delta x_i - x_{ti} - x_{si}}{\Delta y_i - y_{ti} - y_{si}} - \tan^{-1}\frac{\Delta x_i}{\Delta y_i} \tag{30}$$

where $(\Delta x_i, \Delta y_i)$ is the displacement vector,(x_{ti}, y_{ti}) is the translation vector, and (x_{si}, y_{si}) is the zoom vector.

In this work, the zoom scale is set to -7.4175, translation vector is $(-0.6266, -0.6335)$ and rotation angle is 0.7952.

Figure 2 shows the sample image after translation, scaling and rotation. The last image is a superimposed image of each sample. It can be seen that the overlap area is increased in comparison with Fig. 1.

The Level Set Expression of Training Samples. Figure 3 is the zero level set expression of the signed distance function of the contour of each target in the final sample training set.

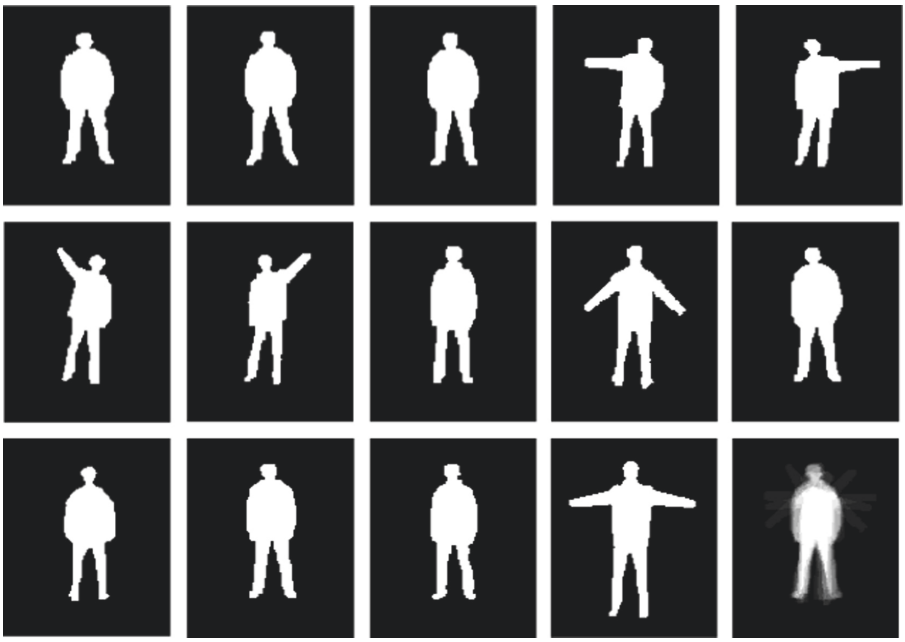

Fig. 2. Human contour's pan and zoom images

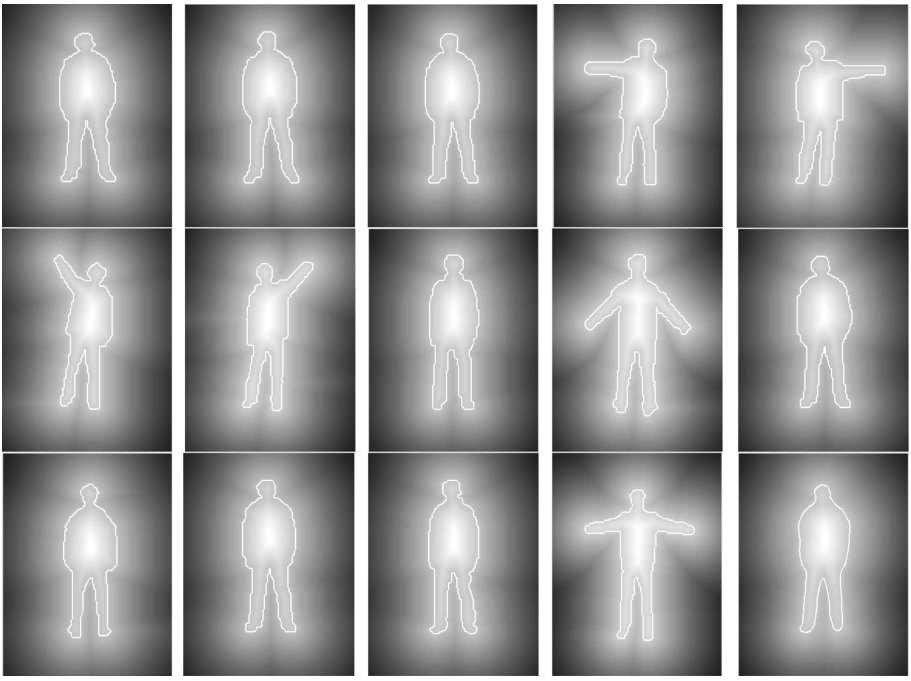

Fig. 3. Level set expression of body contour

Experimental Result. The segmentation process and results of the body using the proposed algorithm is shown in Fig. 4, among which Fig. 4(a) is a 110 × 140 original image. Figure 4(b) is the edge of Fig. 4(a). Figure 4(c) is the initial contour of the level set. Figure 4(d) is the zero level set of the initial contour. Figure 4(f) is the signed distance function of the zero level set. Figure 4(f)–(g) are the process and results of the evolution of the segmentation curve. The red line is the evolution curve, the green line is a priori shape contour curve, and the evolution curve is successfully stopped at the edge of the target after 45 iterations. The model parameters in the Formula (25) are $\mu = 25$, $\alpha = 0.1$, $\beta_1 = \beta_2 = 100$, $\lambda_1 = \lambda_2 = 1.2$, $\lambda = 1.7$, $\gamma = 5$, $\varepsilon = 1$, time step $t = 0.05$.

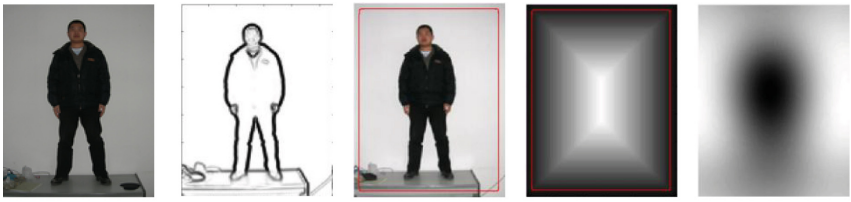

(a) Original image (b) Edge detection (c) Initial contour (d) level set (e) SDF

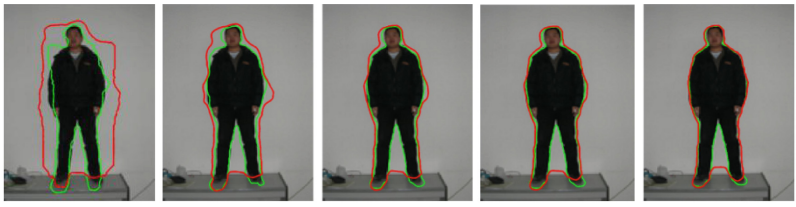

(f) The number of iterations = 2, 4, 6, 8, 10

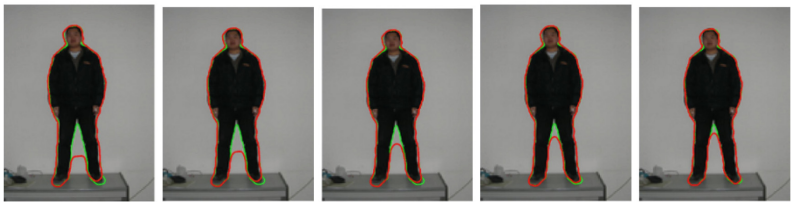

(g) The number of iterations= 15, 17, 20, 35, 45

Fig. 4. Segmentation process and results for human body based on a prior shape

The right lower limb of the segmented object is partially occluded as shown in Fig. 5. Although there is occlusion, the curve after 45 iterations is still successful segmentation, which ensures the integrity of the body.

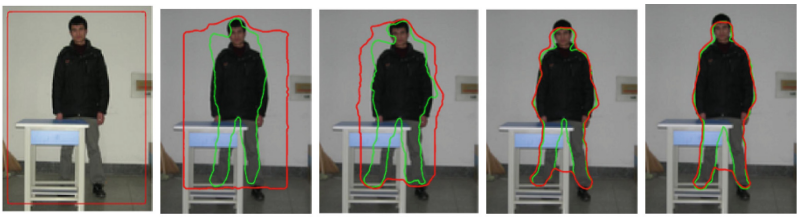

(a) The number of iterations =2，4，6，8，10

(b) The number of iterations = 15，17，20，35，45

Fig. 5. Segmentation process and results for blocked body image based on a prior shape

Figure 6 is the segmentation of the body image polluted by noise and covered partially. Figure 6(a) is a 110 × 140 picture with 0.4 salt pepper noise. Figure 6(b) is the detection edge of Fig. 6(a). Figure 6(c) is the initial contour of the level set, Fig. 6(d) is the zero level set expression of initial contour. Figure 6(e) is signed distance function expression. In Fig. 6(f)–(g), the second row corresponds to the segmentation curve (black) and prior shape curve (green), the curve after 55 iterations successfully stop in the edge of target.

4.2 Segmentation of Ear Contour

As a biometric identification technology, the ear recognition's theory and application research has been paid more attention. The segmentation of ear is also the foundation of recognition [18]. However, the ear's color is similar to skin's, and the part occlusion by ornaments will affect the ear detection and segmentation, thus the shape information is introduced into the level set segmentation model in order to extract the external contour of the ear.

Figure 7 is the segmentation process and results of the blurred image of ear. Figure 7(a) is a 110 × 140 right ear image, the photography equipment jitter leads to ambiguous. As we can see, the white line is the initial contour, and green line is prior shape curve. Although the ear edge is blured in image, prior shape curve can accurately locate near the edge, and the black curve under the guidance of the shape prior reaches the ideal edge.

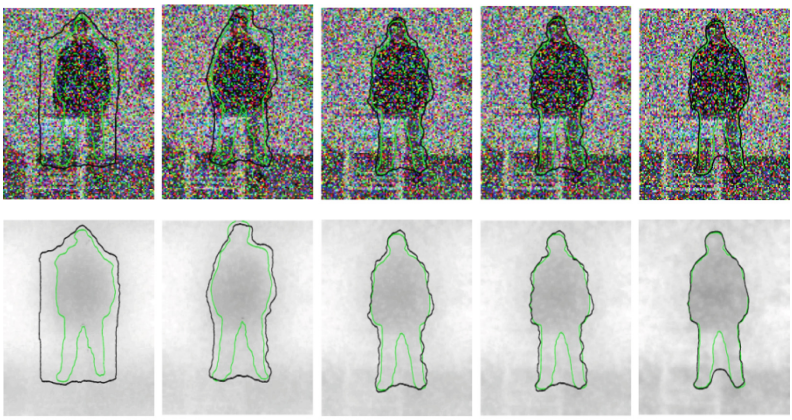

(a) The number of iterations = 2，4，6，8，10

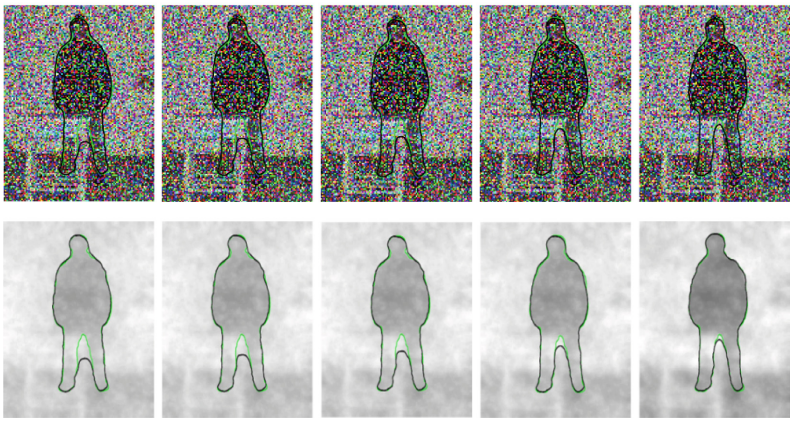

(b) The number of iterations = 15，20，30，40，55

Fig. 6. Segmentation process and results for blocked and noisy body

4.3 Facial Contour Segmentation

Face segmentation has always been a hot topic in the field of image processing. Accurate facial contour segmentation plays a key role in face recognition, facial expression analysis and emotion understanding. Although the scholars have done a lot of research on human face segmentation, the influence of location, light, occlusion and complex background are still the difficulties of solving the problem.

In the first row of Fig. 8, Fig. 8(a) is a 150 × 120 color face image, and Fig. 8(b), Fig. 8(c) and Fig. 8(d) are the results of segmentation using the GAC, model C-V model and the proposed method respectively. Compared with the GAC model and C-V model, the proposed method is better. In the second row, the face is added obstacles as shown in Fig. 8(a), Fig. 8(b) is the segmentation result by the GAC model in 300 iterations, Fig. 8(c) is the result of the 100 iteration by the C-V model, Fig. 8(d) is iterative 5 times results by the proposed method. As we can see, the face can be segmented correctly by the new method.

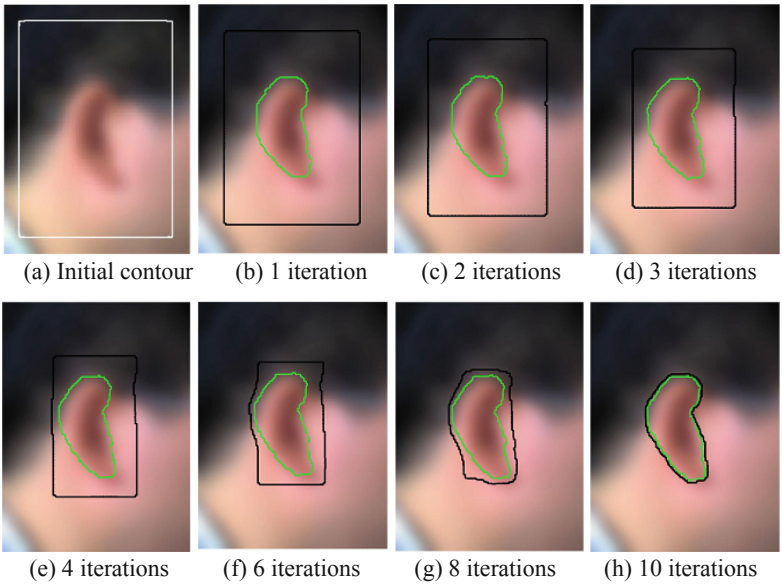

Fig. 7. Segmentation process and results for fuzzy ear based on a prior shape

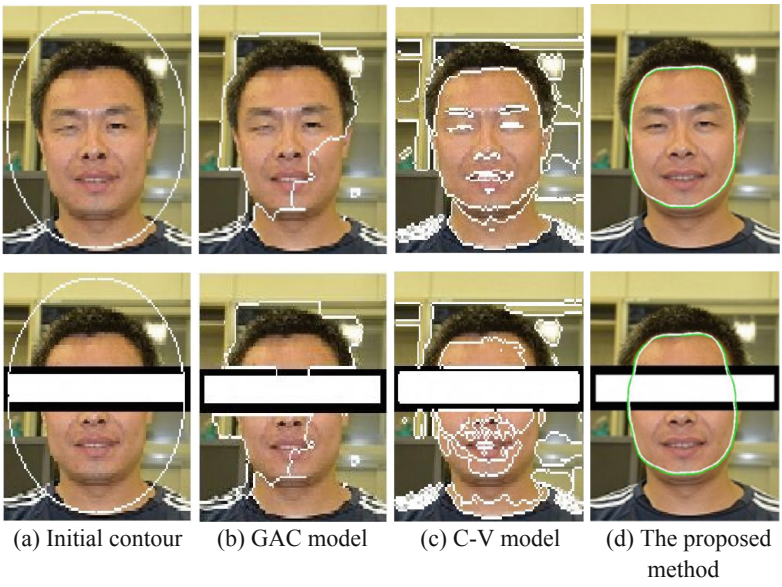

Fig. 8. The results comparison between C-V, GAC and the proposed method

We use the Misclassified Error (ME) as the evaluation method of the experimental results. ME is ratio of number of misclassified pixel and number the object pixel. The smaller value of ME indicates, the better segmentation results is. The ME = 0 shows that

the algorithm is consistent with the manual segmentation results. Through the segmentation of 275 personal face images, experiments show that the segmentation results of C-V model and GAC model are not good, and the ME is 17.3912 and 6.4136 respectively. In contrast, the proposed method can get the ideal segmentation results, the ME is 0.2315 and lower than that of the C-V and GAC model as shown in Table 4.

Table 4. The MEs for the different methods

Segmentation method	Mean error rate
C-V model	17.3912
GAC model	6.4136
The proposed method	0.2315

5 Conclusion

We introduce statistical shape prior information into segmentation model based on level set to improve the robustness of segmentation on biological characteristics. Theoretical analysis and experimental results prove that the proposed method is effective and workable. However, the improved method has some defects to be improved, especially if the background is complex and there are few differences between background and foreground. In addition, the time consuming of the algorithm is increased due to prior shape. Thus future research should focus on improving the robustness, accuracy and efficiency of the algorithm.

Acknowledgments. This Research is funded by the Education Department of Liaoning Province Foundation Grant Number LJQ2014033, the Natural Science Foundation of Liaoning Province Grant Number 20180551048 and the Doctoral Start-up Foundation of Liaoning Province Grant Number 20170520248.

References

1. Afifi, M.: 11K Hands: Gender recognition and biometric identification using a large dataset of hand images. Multimed. Tools Appl. **78**, 20835–20854 (2019). https://doi.org/10.1007/s11042-019-7424-8
2. Sepas-Moghaddam, A., Pereira, F., Correia, P.L.: Ear recognition in a light field imaging framework: a new perspective. IET Biometrics **7**(3), 224–231 (2018)
3. Jain, A.K., Ross, A., Prabhakar, S.: An introduction to biometric recognition. IEEE Trans. Circ. Syst. Video Technol. Spec. Issue Image Video Based Biometrics **14**(1), 4–20 (2004)
4. Eriksson, E., Dan, G., Fodor, V.: Predictive distributed visual analysis for video in wireless sensor networks. IEEE Trans. Mob. Comput. **15**(7), 1743–1756 (2016)
5. Hajdu, A., Kormos, J., Nagy, B., et al.: Choosing appropriate distance measurement in digital image segmentation. Annales Univ. Sci. Budapest. Sec. Comp. **24**, 193–208 (2004)

6. Paragios, N., Chen, Y., Faugeras, O. (eds.): Handbook of Mathematical Models in Computer Vision. Springer, New York (2006). https://doi.org/10.1007/0-387-28831-7
7. Dockins, K.: Template method. In: Design Patterns in PHP and Laravel (2017)
8. Kuang, H., Cai, S., Ma, X., et al.: An effective skeleton extraction method based on kinect depth image. In: International Conference on Measuring Technology & Mechatronics Automation (2018)
9. Leventon, M.E., Grimson, W.E.L., Faugeras, O.: Statistical shape influence in geodesic active contours. In: Proceedings of the IEEE Conference on Compute Vision Pattern Recognition, vol. 1, pp. 316–323 (2000)
10. Rousson, M., Paragios, N.: Shape priors for level set representations. In: Heyden, A., Sparr, G., Nielsen, M., Johansen, P. (eds.) ECCV 2002. LNCS, vol. 2351, pp. 78–92. Springer, Heidelberg (2002). https://doi.org/10.1007/3-540-47967-8_6
11. Pan, B., Wang, W., Yan, J., et al.: For prostate MRI segmentation: a prior-shape-based level set model combined with gradient and regional information. In: 2018 IEEE International Conference on Mechatronics and Automation (ICMA) (2018)
12. Cremers, D., Tischhauser, E., Weickert, J., Schnorr, C.: Diffusion snakes: introducing statistical shape knowledge into the Mumford-Shah functional. Int. J. Comput. Vis. **50**(3), 295–3133 (2002)
13. Cremers, D., Sochen, N., Schnorr, C.: A multiphase dynamic labeling model for variational recognition-driven image segmentation. Int. J. Comput. Vis. **66**(1), 67–81 (2006)
14. Karantzalos, K., Paragios, N.: Recognition-driven two-dimensional competing priors toward automatic and accurate building detection. IEEE Trans. Geosci. Remote Sens. **47**(1), l33-144 (2009)
15. Karantzalos, K., Paragios, N.: Large-scale building reconstruction through information fusion and 3-D priors. IEEE Trans. Geosci. Remote Sens. **48**(5), 2283–2296 (2010)
16. Cootes, T.F., Taylor, C.J., Cooper, D.H., Grahan, J.: Active shape models their training and application. Comput. Vis. Image Underst. **61**(1), 38–59 (1995)
17. Wong, A.K.C., Liu, T.S.: Typicality, diversity, and feature pattern of an ensemble. IEEE Trans. Comput. **24**(2), 158–181 (1975)
18. Emersic, Z., Gabriel, L.L., Struc, V., et al.: Convolutional encoder-decoder networks for pixel-wise ear detection and segmentation. IET Biometrics **7**(3), 175–184 (2018)